Editors' Suggestion

Quantum Critical Behavior of Entanglement in Lattice Bosons with Cavity-Mediated Long-Range Interactions

Shraddha Sharma,[1,2,*] Simon B. Jäger,[1,3,4,*] Rebecca Kraus,[1] Tommaso Roscilde,[5] and Giovanna Morigi[1]
[1]Theoretische Physik, Saarland University, Campus E2.6, 66123 Saarbrücken, Germany
[2]ICTP—The Abdus Salam International Center for Theoretical Physics, Strada Costiera 11, 34151 Trieste, Italy
[3]Physics Department and Research Center OPTIMAS, Technische Universität Kaiserslautern, D-67663, Kaiserslautern, Germany
[4]JILA and Department of Physics, University of Colorado, 440 UCB, Boulder, Colorado 80309, USA
[5]Univ. Lyon, Ens de Lyon, CNRS, Laboratoire de Physique, F-69342 Lyon, France

(Received 25 April 2022; accepted 2 September 2022; published 26 September 2022)

We analyze the ground-state entanglement entropy of the extended Bose-Hubbard model with infinite-range interactions. This model describes the low-energy dynamics of ultracold bosons tightly bound to an optical lattice and dispersively coupled to a cavity mode. The competition between on-site repulsion and global cavity-induced interactions leads to a rich phase diagram, which exhibits superfluid, supersolid, and insulating (Mott and checkerboard) phases. We use a slave-boson treatment of harmonic quantum fluctuations around the mean-field solution and calculate the entanglement entropy across the phase transitions. At commensurate filling, the insulator-superfluid transition is signaled by a singularity in the area-law scaling coefficient of the entanglement entropy, which is similar to the one reported for the standard Bose-Hubbard model. Remarkably, at the continuous $\mathbb{Z}_2$ superfluid-to-supersolid transition we find a *critical* logarithmic term, regardless of the filling. This behavior originates from the appearance of a roton mode in the excitation and entanglement spectrum, becoming gapless at the critical point, and it is characteristic of collective models.

DOI: 10.1103/PhysRevLett.129.143001

Introduction.—Entanglement measures play a special role in the low-temperature physics of quantum many-body systems, as they probe the existence and structure of quantum correlations [1]. Different entanglement measures have been discussed and applied to classify the emerging states of quantum matter [1,2]. Among them, entanglement entropy (EE) captures the presence of bipartite entanglement in pure states: the scaling of the EE of a connected subsystem with its size exhibits universal properties [3–5] probing, e.g., the presence of conventional long-range order [6], or of topological order [7,8]. Singularities in the scaling behavior of the EE can mark in a universal way quantum phase transitions separating ordered from disordered phases [9–12].

In this Letter, we focus on the von Neumann EE, S, for a spatial bipartition $\mathbb{A}$ and $\mathbb{B}$ of an extended quantum system:

$$S = -\mathrm{Tr}\{\rho_{\mathbb{A}} \log \rho_{\mathbb{A}}\}, \tag{1}$$

where $\rho_{\mathbb{A}} = \mathrm{Tr}_{\mathbb{B}}\{|\Psi_0\rangle\langle\Psi_0|\}$ is the density matrix obtained by tracing out the degrees of freedom of subsystem $\mathbb{B}$ from the ground state $|\Psi_0\rangle$. Our purpose is to characterize the scaling of S at continuous phase transitions resulting from competing short- and global-range interactions.

In fact, the interaction range can give rise to very different entanglement features. For short-range interactions the dominant scaling term of the EE is the so-called area-law term. This term grows with the size of the boundary between $\mathbb{A}$ and $\mathbb{B}$. For a lattice of d dimensions and L lattice sites along each spatial dimension the total number of lattice sites is $N = L^d$, and the EE scales as L^{d-1} for a connected subsystem $\mathbb{A}$ [3]. This area-law scaling can be taken as an indication that quantum correlations between $\mathbb{A}$ and $\mathbb{B}$ involve primarily lattice sites close to the boundary [13]; yet, for bosonic or spin systems in $d > 1$ dimensions it persists even for ground states

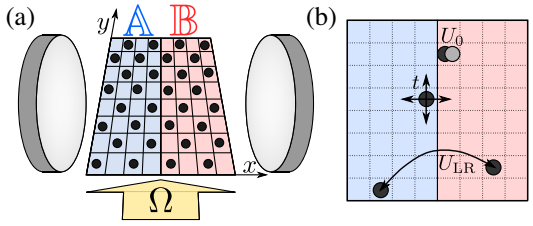

FIG. 1. The Bose-Hubbard model with competing short and global interactions can be realized with atoms tightly bound by an optical lattice that coherently scatters laser photons (Ω) into the mode of a high-finesse cavity [26]. (a) The picture shows the geometry of the $\mathbb{A}/\mathbb{B}$ bipartition considered in this Letter. (b) Illustration of competing processes of the Hamiltonian: the nearest-neighbor tunneling (with amplitude t), the on site repulsion (U_0), and the global density-density interactions (U_{LR}), which are attractive here.

exhibiting critical or long-range correlations associated with the spontaneous breaking of a continuous symmetry [14–16]. In fact, criticality may lead at most to a singularity in the coefficient of the area-law scaling [11,13,17,18], while long-range correlations lead to the appearance of a universal subleading contribution to EE scaling. This contribution scales with the number of Goldstone modes N_G as $(N_G/2)(d-1)\log L$ [6]. In contrast, for long-range interactions that decay with the interparticle distance r as $1/r^\alpha$ with $\alpha < d$, the geometric boundary between $\mathbb{A}$ and $\mathbb{B}$ becomes unimportant [19–21]. For example, the area-law scaling disappears in the Dicke [22] and the Lipkin-Meshkov-Glick (LMG) model [23–25]. Here, the ground state belongs to a symmetric subspace whose dimension grows linearly with N, and the EE scales as $\log(N)$ at the quantum critical point [9]. To our knowledge, the scaling behavior of the EE is unexplored in the regime where short-range and global interactions compete.

Extended Bose-Hubbard model.—In this Letter we analyze the scaling of the EE in the two-dimensional extended Bose-Hubbard model of cavity quantum electrodynamics [26–29]—see Fig. 1 for a sketch. The Hamiltonian is the sum of the standard Bose-Hubbard Hamiltonian $\hat{H}_{\mathrm{BH}}$ [30] and the cavity-mediated long-range interaction potential $\hat{H}_{\mathrm{cav}}$, namely, $\hat{H} = \hat{H}_{\mathrm{BH}} + \hat{H}_{\mathrm{cav}}$, with

$$\hat{H}_{\mathrm{BH}} = -t\sum_{\langle \boldsymbol{r},\boldsymbol{r}'\rangle} \hat{b}^\dagger_{\boldsymbol{r}}\hat{b}_{\boldsymbol{r}'} + \sum_{\boldsymbol{r}}\left[\frac{U_0}{2}\hat{n}_{\boldsymbol{r}}(\hat{n}_{\boldsymbol{r}}-1) - \mu\hat{n}_{\boldsymbol{r}}\right], \quad (2)$$

$$\hat{H}_{\mathrm{cav}} = -\frac{U_{\mathrm{LR}}}{N}\left[\sum_{\boldsymbol{r}}(-1)^{r_x+r_y}\hat{n}_{\boldsymbol{r}}\right]^2, \quad (3)$$

where the parameters t, U_0, and U_{LR} are real and positive; $\hat{b}^\dagger_{\boldsymbol{r}}$ ($\hat{b}_{\boldsymbol{r}}$) create (annihilate) a boson at the site $\boldsymbol{r} = (r_x, r_y)$ of the square lattice; $\hat{n}_{\boldsymbol{r}} = \hat{b}^\dagger_{\boldsymbol{r}}\hat{b}_{\boldsymbol{r}}$ is the density, and $\langle \boldsymbol{r},\boldsymbol{r}'\rangle$ indicates a pair of nearest neighbors. In the following we assume periodic boundary conditions.

Theoretical studies of the phase diagram of the Hamiltonian $\hat{H}$ [28,29,31–35] reproduce the experimental results of Ref. [26] for a cavity wavelength which is twice the periodicity of the optical lattice. This ground-state phase diagram features a rich palette of phases: The nearest-neighbor hopping with amplitude t favors the onset of superfluidity (SF) while the on-site repulsion, with amplitude U_0, stabilizes a Mott insulator (MI) at commensurate filling. Global interactions, with amplitude U_{LR}, induce a density modulation which supports scattering of photons into the cavity field. The density modulation can result either in a charge density-wave (CDW) insulator, at integer or half-integer filling, or a supersolid (SS) phase, when it also exhibits superfluidity. Experimentally, the condensate fraction is revealed by time-of-flight measurements, while the onset of diagonal long-range order leads to the emission of coherent light at the cavity output [26,36].

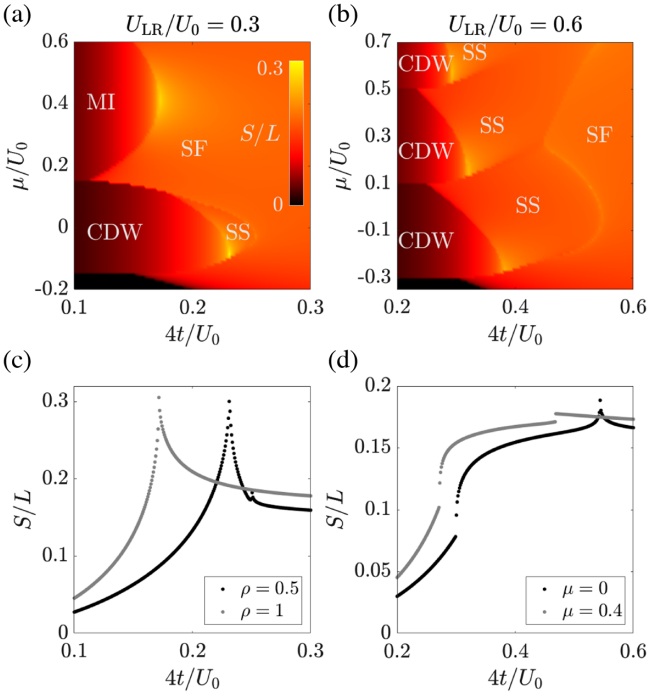

FIG. 2. Color plot of the half-system EE S [Eq. (1)] [see the partition in Fig. 1(a)] for (a) $U_{\mathrm{LR}}/U_0 = 0.3$ and (b) $U_{\mathrm{LR}}/U_0 = 0.6$ as functions of the tunneling t and the chemical potential μ in units of U_0 for a $L \times L$ square lattice with $L = 40$. The nonanalyticities of S coincide with the phase transition lines predicted by mean-field theory (not indicated here). The lower panels show S/L as a function of t/U_0 (c) at fixed density ρ for $U_{\mathrm{LR}} = 0.3U_0$; and (d) at fixed chemical potential μ/U_0 for $U_{\mathrm{LR}} = 0.6U_0$. Here the system the size is $L = 60$.

The phase diagram is theoretically determined in the grand-canonical ensemble via the Gutzwiller mean-field (MF) approach [35]. The ground state is written in the spatially factorized form $|\Psi_{0,\mathrm{MF}}\rangle = \otimes_{\boldsymbol{r}} |\psi_{\boldsymbol{r},0}\rangle$ with $|\psi_{\boldsymbol{r},0}\rangle = \sum_{n=0}^{n_{\max}} f^{(0)}_{\boldsymbol{r},n}|n\rangle_{\boldsymbol{r}}$, where $|n\rangle_{\boldsymbol{r}}$ are the single-site Fock states and $n_{\max}$ is a cutoff, chosen to be $n_{\max} = 6$ throughout this Letter, and leading to negligible truncation errors. The single-particle state $|\psi_{\boldsymbol{r},0}\rangle$ is the ground state of the effective single-site Hamiltonian $\hat{H}^{\mathrm{MF}}_{\boldsymbol{r}}$, and it is determined self-consistently. Here, $\hat{H}^{\mathrm{MF}}_{\boldsymbol{r}} = -zt\bar{\varphi}_{\boldsymbol{r}}(\hat{b}_{\boldsymbol{r}} + \hat{b}^\dagger_{\boldsymbol{r}} - \varphi_{\boldsymbol{r}}) + (U_0/2)\hat{n}_{\boldsymbol{r}}(\hat{n}_{\boldsymbol{r}}-1) - \mu\hat{n}_{\boldsymbol{r}} - U_{\mathrm{LR}}\Theta(-1)^{r_x+r_y}\hat{n}_{\boldsymbol{r}} + NU_{\mathrm{LR}}\Theta^2/4$ where z is the lattice coordination number ($z = 4$) [35]. Superfluidity is signaled by a nonvanishing value of the order parameter $\bar{\varphi}_{\boldsymbol{r}} = \sum_{\boldsymbol{r}'}\varphi_{\boldsymbol{r}'}/z$, where $\varphi_{\boldsymbol{r}} = \langle \hat{b}_{\boldsymbol{r}}\rangle$ and the sum runs over the nearest neighbors $\boldsymbol{r}'$ of $\boldsymbol{r}$. The onset of a density modulation is revealed by the order parameter $\Theta = 2\langle\sum_{\boldsymbol{r}}(-1)^{r_x+r_y}\hat{n}_{\boldsymbol{r}}\rangle/N$. The upper panels of Fig. 2 display the phase diagram as a function of the ratios t/U_0 and μ/U_0, and the color scale gives the value of the EE, whose determination is discussed below. The subplots are evaluated for two values of the global potential U_{LR}, chosen (a) below and (b) above the threshold $U^{\mathrm{th}}_{\mathrm{LR}} = U_0/2$, at which the MI phase becomes unstable.

The nonanalyticities of the EE coincide with the mean-field phase boundaries of Ref. [35].

The phase diagram features first-order phase transitions and three main types of *continuous* quantum phase transitions [28,34,35]. The first type (type 1) is a commensurate O(2) phase transition, separating either the MI from the SF at fixed integer density ρ, or the CDW from the SS at fixed integer density and at half filling. This transition occurs at the tip of the corresponding (MI or CDW) lobe. The second type (type 2) is a generic transition separating MI from SF and CDW from SS at incommensurate densities. This appears everywhere along the borders separating either MI-SF or CDW-SS, except for the lobe tips. The third type (type 3) is a continuous $\mathbb{Z}_2$ transition between the SS and the SF phase. Some of these phase transitions change in fact from continuous to first order as the t/U_0 and μ/U_0 ratios are tuned across the phase diagram. This is the case at the CDW-SS and SS-SF for small t/U_0, and at the SS-SF transition for $\mu/U_0 \gtrsim 0.25$ [see Fig. 2(b)]. We note that phase transitions changing from continuous to discontinuous as a function of the control fields (or the temperature) have also been reported for spin systems with competing short and long-range interactions [19,37].

Slave-boson approach.—We determine the entanglement properties in this rich phase diagram by including quantum correlations which are not captured by the MF approximation. For this purpose we make use of a slave-boson approach [11,38], which we outline below and detail in the Supplemental Material [39]. Such an approach consists of using the full basis $\{|\psi_{\boldsymbol{r},\alpha}\rangle\}$ of eigenstates of $H_{\boldsymbol{r}}^{\mathrm{MF}}$ $(\alpha = 0, \ldots, n_{\max})$, and of defining associated slave-boson operators $\hat{\gamma}_{\boldsymbol{r},\alpha}$, $\hat{\gamma}_{\boldsymbol{r},\alpha}^{\dagger}$. These operators fulfill the hardcore constraint $\sum_{\alpha} \hat{\gamma}_{\boldsymbol{r},\alpha}^{\dagger}\hat{\gamma}_{\boldsymbol{r},\alpha} = 1$ and are used to rewrite the original bosonic operators $\hat{b}_{\boldsymbol{r}} = \sum_{\alpha\beta}\sum_{n}\sqrt{n} f_{\boldsymbol{r},n-1}^{(\alpha)} f_{\boldsymbol{r},n}^{(\beta)} \hat{\gamma}_{\boldsymbol{r},\alpha}^{\dagger}\hat{\gamma}_{\boldsymbol{r},\beta}$ in $\hat{H}$. Within this formalism, the MF approximation corresponds to the condensation hypothesis of the ground-state slave bosons, $\hat{\gamma}_{\boldsymbol{r},0}, \hat{\gamma}_{\boldsymbol{r},0}^{\dagger} = 1$ and $\langle \hat{\gamma}_{\boldsymbol{r},\alpha>0}^{\dagger}\hat{\gamma}_{\boldsymbol{r},\alpha>0}\rangle = 0$. The next level of approximation is to retain a finite population for the $\alpha > 0$ bosons, and truncate the full quartic Hamiltonian $\hat{H}$ to quadratic order in the $\hat{\gamma}_{\boldsymbol{r},\alpha>0}$, $\hat{\gamma}_{\boldsymbol{r},\alpha>0}^{\dagger}$ operators, by assuming that $\langle \hat{\gamma}_{\boldsymbol{r},\alpha>0}^{\dagger}\hat{\gamma}_{\boldsymbol{r},\alpha>0}\rangle \ll 1$ and $\hat{\gamma}_{\boldsymbol{r},0}, \hat{\gamma}_{\boldsymbol{r},0}^{\dagger} \approx (1 - \sum_{\alpha>0}\hat{\gamma}_{\boldsymbol{r},\alpha}^{\dagger}\hat{\gamma}_{\boldsymbol{r},\alpha})^{1/2}$. The resulting Hamiltonian then reads as $\hat{H} \approx \langle \Psi_{0,\mathrm{MF}}|\hat{H}|\Psi_{0,\mathrm{MF}}\rangle + \hat{H}^{(2)}$ where $\hat{H}^{(2)}$ is a quadratic form in $\hat{\gamma}_{\boldsymbol{r},\alpha>0}$, $\hat{\gamma}_{\boldsymbol{r},\alpha>0}^{\dagger}$ operators [39]. A Bogolyubov diagonalization of $\hat{H}^{(2)}$ reconstructs the quasiparticle spectrum $\omega_{\boldsymbol{k},p}$ (where p is a mode index, $p = 1, \ldots, n_{\max}$), and it allows us to calculate the covariance matrix for subsystem $\mathbb{A}$, $\mathbf{C}_{\mathbb{A}} = [\mathbf{C}_{\boldsymbol{r},\boldsymbol{r}'}]_{\boldsymbol{r},\boldsymbol{r}'\in\mathbb{A}}$, where $\mathbf{C}_{\boldsymbol{r},\boldsymbol{r}'} = \langle\Psi_0|(\hat{\boldsymbol{\gamma}}_{\boldsymbol{r}}, \hat{\boldsymbol{\gamma}}_{\boldsymbol{r}}^{\dagger})^T(\hat{\boldsymbol{\gamma}}_{\boldsymbol{r}'}^{\dagger}, \hat{\boldsymbol{\gamma}}_{\boldsymbol{r}'})|\Psi_0\rangle$ with $\hat{\boldsymbol{\gamma}}_{\boldsymbol{r}} = (\hat{\gamma}_{\boldsymbol{r},1}, \hat{\gamma}_{\boldsymbol{r},2}, \ldots)$. For the remainder of this Letter, $\mathbb{A}$ will be the $L/2 \times L$ rectangle obtained by cutting the $L \times L$ square lattice along the y coordinate axis. The matrix $\mathbf{C}_{\mathbb{A}}$ contains all the information on the Gaussian reduced density matrix $\hat{\rho}_{\mathbb{A}} = e^{-\hat{H}_{\mathbb{A}}}$ for subsystem $\mathbb{A}$. Operator $\hat{H}_{\mathbb{A}}$ is the so-called entanglement Hamiltonian, and it is a quadratic form in the $\hat{\gamma}_{\boldsymbol{r},\alpha>0}$, $\hat{\gamma}_{\boldsymbol{r},\alpha>0}^{\dagger}$. By means of a Bogolyubov transformation $\hat{H}_{\mathbb{A}}$ becomes diagonal,

$$\hat{H}_{\mathbb{A}} = \sum_{k_y,m} \lambda_{k_y,m} \hat{d}_{k_y,m}^{\dagger}\hat{d}_{k_y,m}, \tag{4}$$

where $\hat{d}_{k_y,m}$, $\hat{d}_{k_y,m}^{\dagger}$ are bosonic operators, $\lambda_{k_y,m}$ represents the so-called (one-particle) entanglement spectrum, and we dropped a constant term. The entanglement spectrum is labeled by the wave vector k_y along the cut and by a further mode index m associated with the motion perpendicular to the cut. The EE S corresponds then to the entropy of a gas of free bosons whose dispersion relation is the entanglement spectrum: $S = \sum_{k_y,m} s(n_{k_y,m})$ where $s(x) = (1+x)\log(1+x) - x\log x$ and $n_{k_y,m} = [\exp(\lambda_{k_y,m}) - 1]^{-1}$ is the Bose distribution.

Entanglement phase diagram.—Figures 2(a) and 2(b) display S in false colors throughout the phase diagrams. Remarkably, the EE exhibits characteristic signatures at *all* quantum phase transitions. In Fig. 2(c) we report representative cuts at fixed density $\rho = 1/2$ and $\rho = 1$ for $U_{\mathrm{LR}}/U_0 = 0.3$. These cuts show the existence of a sharp cusp singularity at the O(2) MI-SF and CDW-SS transition (type 1). This singularity is associated with the appearance of a Higgs-like mode in the entanglement spectrum becoming gapless at the transition, and reflecting the softening of the Higgs mode in the quasiparticle spectrum [43]. The vanishing of the gap of the Higgs-like mode gives a singular contribution to the dominant, area-law scaling term. This behavior was reported in Ref. [11] for the MI-SF transition in the standard Bose-Hubbard model; and it also characterizes the CDW-SS transition (see the Supplemental Material [39]). For the continuous generic MI-SF and CDW-SS transition (type 2), occurring away from the lobe tips in Figs. 2(a) and 2(b), the EE singularity turns into a rounded maximum, similarly to the behavior of the standard Bose-Hubbard model [11]. In the extended Bose-Hubbard model, therefore, the critical behavior of entanglement at these phase transitions (type 1 and type 2) is due to the competition between hopping and contact short-range interactions. The singularity of entanglement entropy for a transition of type 1 has been analyzed in Ref. [11].

On the contrary, the long-range interactions play a crucial role for the continuous $\mathbb{Z}_2$ SS-SF transition (type 3) and its entanglement properties, as we argue below. We generally observe a smaller cusplike singularity of the EE at this transition. This is visible in the transition at fixed chemical potential ($\mu = 0$) in Fig. 2(d) as well as in the transition at constant density ($\rho = 1/2$) in Fig. 2(c). In fact, the cusp singularity marks the *entire* SS-SF boundary

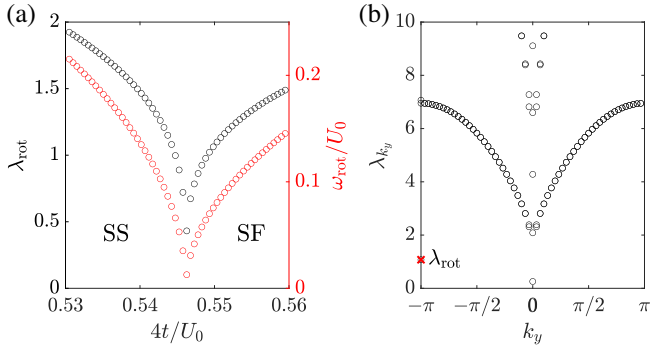

FIG. 3. (a) The roton-mode frequencies $\lambda_{\rm rot} = \lambda_{\pi,\bar{m}}$ ($\bar{m}$ being the index of the rotonlike mode) and $\omega_{\rm rot}$ in the entanglement and physical spectrum (respectively) as a function of $4t/U_0$ across the SS-SF phase transition. Both frequencies vanish at the SS-SF transition. (b) Entanglement spectrum for $4t = 0.55U_0$, $U_{\rm LR} = 0.6U_0$, $\mu = -0.05U_0$, and $L = 60$ as functions of k_y. The roton mode in the entanglement spectrum is highlighted by the red cross.

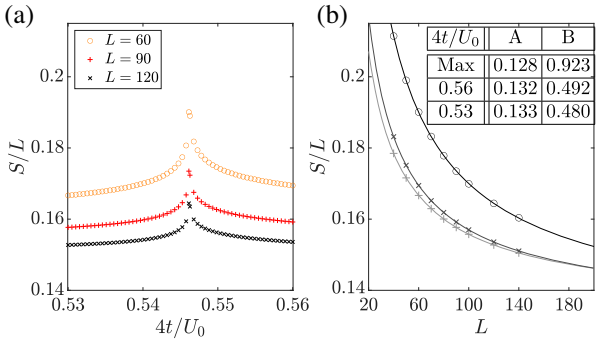

FIG. 4. The half-system EE as a function of the tunneling rate t in units of U_0 across the transition from SS-SF, for $U_{\rm LR} = 0.6U_0$ and constant $\mu = -0.05U_0$. (b) Scaling of the S/L values at the maximum ("o" symbols), for $4t/U_0 = 0.56$ ("x" symbols), and for $4t/U_0 = 0.53$ ("+" symbols) for different L. The coefficients A and B are obtained by fitting Eq. (5) to S vs L and are given in the table. For all the data in this figure the scaling exponent of the regularizing field $h(L)$ has been chosen as $\kappa = 4$.

whenever the corresponding transition is continuous. This cusp behavior can be well distinguished from the singularity at the MI-SF and CDW-SS transitions and originates from a singularity in the log correction of the EE, as we shall explain later. The robustness of this singularity in the EE makes the SS-SF transition stand out with respect to the MI-SF and the CDW-SS transitions of the same model, and it represents our most important finding. Finally, when the transitions are first order, the EE becomes discontinuous. This is visible in Fig. 2(d) for the CDW-SS and the SS-SF transition at the constant value of the chemical potential $\mu = 0.4U_0$.

Entanglement singularity from the roton mode.—To understand the origin of the cusp singularity at the SS-SF transition, it is useful to analyze the behavior of the excitation spectrum at the SS-SF transition. The spectrum exhibits a vanishing gap throughout the SF and SS phase, coming from the Goldstone mode related to the breaking of the U(1) symmetry. Moreover, it is characterized by the critical softening of the roton frequency $\omega_{\rm rot}$ at wave vector $\boldsymbol{k}_{\rm rot} = (\pi, \pi)$ [28], which is the precursor of diagonal long-range order. The roton gap is displayed in Fig. 3(a) as a function of t/U_0. After closing at the SS-SF transition it reopens in the SS phase: this is a consequence of elementary excitations of a $\mathbb{Z}_2$ crystal having a finite, nonvanishing gap just like in the CDW phase. The spectrum has a characteristic *dispersionless* and gapped structure in the vicinity of the critical roton mode at $\boldsymbol{k}_{\rm rot}$, reflecting the fact that the Fourier spectrum of the global interaction potential is a δ function at this wave vector. Correspondingly, in the entanglement spectrum [Fig. 3(b)], a (boundary) rotonlike mode becomes gapless only at the SS-SF transition, and only for the frequency $\lambda_{\rm rot}$. This means that the EE acquires the critical roton contribution $S_{\rm rot} = s(n_{\rm rot}) \approx -\log \lambda_{\rm rot}$ as $\lambda_{\rm rot} \to 0$.

The scaling of the critical roton contribution with system size L depends then on how the roton entanglement frequency $\lambda_{\rm rot}$ vanishes upon increasing L. This shall be handled with particular care. In fact, diagonalization of the quadratic Hamiltonian $\hat{H}^{(2)}$ leads to the unphysical result that the frequency $\omega_{\rm rot}$ vanishes for any finite system size at the SS-SF transition (and so does the frequency $\lambda_{\rm rot}$ of the entanglement spectrum). This is a common problem for the treatment of harmonic quantum fluctuations around a symmetry-breaking mean-field solution. In order to have meaningful finite-size results, we implement a regularization scheme by applying a size-dependent field. This field couples to the order parameter and introduces a finite gap both in the excitation as well as in the entanglement spectrum [40,44]. For the $\mathbb{Z}_2$ critical point with infinite-range interactions, we add a term $-h(L)\sum_{\boldsymbol{r}}(-1)^{\boldsymbol{r}} n_{\boldsymbol{r}}$ with $h(L) \sim L^{-\kappa}$. This choice is such that the gap introduced in the "zero-modes" mimics the scaling of the excitation gap at the transition $\omega_{\rm rot} \sim L^{-z}$, with z the dynamical critical exponent. The size-dependent field $h(L)$ also introduces a finite-size scaling for the entanglement frequency $\lambda_{\rm rot} \sim L^{-\zeta}$. The determination of the scaling exponent κ reproducing the correct z exponent goes beyond the scope of our Letter. Yet, even though different power-law scalings of the applied field lead to different scalings $\lambda_{\rm rot} \sim L^{-\zeta(\kappa)}$ for the roton mode, all choices result in a singular logarithmic correction to the area law of the form $S_{\rm rot} \simeq \zeta \log L$.

Scaling of the EE.—We perform a scaling analysis of the half-system EE using the fitting function

$$S = AL + B\log L + C. \tag{5}$$

Figure 4 clearly shows that the spike in the EE at the transition is due to a spike in the fitted B coefficient. This spike appears on top of the value $B \approx N_G(d-1)/2 = 1/2$ related to the contribution of the Goldstone mode, and is

consistent with the singular logarithmic contribution to the EE coming from the roton mode. This is revealed by plotting S/L vs L: the curves at the critical point or away from it tend to a similar A value—the area-law scaling term—but are offset sharply by the spike in the subleading term $B \log L/L$. It is interesting to frame this result in the broader context of quantum phase transitions in models with global interactions [9]. In the Supplemental Material [39] we show that a slave-boson treatment of the LMG model recovers exactly the $\log N$ scaling behavior of the EE at the critical point. We relate this behavior quantitatively to the appearance of an isolated vanishing mode $\lambda_{\min}$ in an otherwise nearly dispersionless entanglement spectrum.

Conclusions.—We have shown that the EE sheds light on the role of the interaction range at the quantum phase transitions of the extended Bose-Hubbard model of cavity quantum electrodynamics (CQED). The continuous phase transitions separating the insulating from the superfluid phases exhibit a singularity in the coefficient of the area-law scaling of the EE, as in the short-range Bose-Hubbard model. Remarkably, at the continuous $\mathbb{Z}_2$ superfluid-supersolid transition, the EE's behavior is accompanied by a critical logarithmic scaling term of the EE, originating from the singular vanishing of the roton gap. The behavior of a vanishing gap in a dispersionless roton mode is similar to the one reported at the quantum phase transition of collective spin models and is determined by the global-range potential. This analysis can be extended to characterize quantum phase transitions of driven-dissipative CQED models [45–47]. The perspective of studying cavity-induced correlations in quantum gas microscopes [48] opens the possibility of measuring EE via the replica [49] or the random-measurement approach [50], and it suggests that our predictions could be accessible to future experiments.

The authors are grateful to Irénée Frérot, Lukas Himbert, and Astrid Elisabeth Niederle for discussions and helpful comments. This work has been supported by the Deutsche Forschungsgemeinschaft (DFG, German Research Foundation) via the priority program No. 1929 "GiRyd" and the CRC-TRR 306 "QuCoLiMa, Quantum Cooperativity of Light and Matter," Project-ID No. 429529648, and by the German Ministry of Education and Research (BMBF) via the QuantERA project NAQUAS. Project NAQUAS has received funding from the QuantERA ERA-NET Cofund in Quantum Technologies implemented within the European Union's Horizon 2020 program. S. B. J. acknowledges support from the NSF Q-SEnSE Grant No. OMA 2016244, NSF PFC Grant No. 1734006, and from Research Centers of the Deutsche Forschungsgemeinschaft (DFG): Projects A4 and A5 in SFB/Transregio 185: "OSCAR." T. R. acknowledges support from ANR (EELS project) and QuantERA (MAQS project).

[*] These authors contributed equally to this work.

[1] L. Amico, R. Fazio, A. Osterloh, and V. Vedral, Rev. Mod. Phys. **80**, 517 (2008).
[2] R. Horodecki, P. Horodecki, M. Horodecki, and K. Horodecki, Rev. Mod. Phys. **81**, 865 (2009).
[3] J. Eisert, M. Cramer, and M. B. Plenio, Rev. Mod. Phys. **82**, 277 (2010).
[4] M. B. Plenio, J. Eisert, J. Dreißig, and M. Cramer, Phys. Rev. Lett. **94**, 060503 (2005).
[5] M. Cramer, J. Eisert, and M. B. Plenio, Phys. Rev. Lett. **98**, 220603 (2007).
[6] M. A. Metlitski and T. Grover, arXiv:1112.5166.
[7] M. Levin and X.-G. Wen, Phys. Rev. Lett. **96**, 110405 (2006).
[8] A. Kitaev and J. Preskill, Phys. Rev. Lett. **96**, 110404 (2006).
[9] J. Vidal, S. Dusuel, and T. Barthel, J. Stat. Mech. (2007) P01015.
[10] P. Calabrese and J. Cardy, J. Phys. A **42**, 504005 (2009).
[11] I. Frérot and T. Roscilde, Phys. Rev. Lett. **116**, 190401 (2016).
[12] F. Lingua, A. Richaud, and V. Penna, Entropy **20**, 84 (2018).
[13] V. Alba, M. Haque, and A. M. Läuchli, Phys. Rev. Lett. **110**, 260403 (2013).
[14] H. Casini and M. Huerta, J. Phys. A **42**, 504007 (2009).
[15] M. B. Hastings, I. González, A. B. Kallin, and R. G. Melko, Phys. Rev. Lett. **104**, 157201 (2010).
[16] S. Humeniuk and T. Roscilde, Phys. Rev. B **86**, 235116 (2012).
[17] R. R. P. Singh, R. G. Melko, and J. Oitmaa, Phys. Rev. B **86**, 075106 (2012).
[18] J. Helmes and S. Wessel, Phys. Rev. B **89**, 245120 (2014).
[19] A. Campa, T. Dauxois, and S. Ruffo, Phys. Rep. **480**, 57 (2009).
[20] Z.-X. Gong, M. Foss-Feig, F. G. S. L. Brandão, and A. V. Gorshkov, Phys. Rev. Lett. **119**, 050501 (2017).
[21] T. Kuwahara and K. Saito, Nat. Commun. **11**, 4478 (2020).
[22] K. Hepp and E. H. Lieb, Ann. Phys. (N.Y.) **76**, 360 (1973).
[23] H. Lipkin, N. Meshkov, and A. Glick, Nucl. Phys. **62**, 188 (1965).
[24] N. Meshkov, A. Glick, and H. Lipkin, Nucl. Phys. **62**, 199 (1965).
[25] A. Glick, H. Lipkin, and N. Meshkov, Nucl. Phys. **62**, 211 (1965).
[26] R. Landig, L. Hruby, N. Dogra, M. Landini, R. Mottl, T. Donner, and T. Esslinger, Nature (London) **532**, 476 (2016).
[27] H. Habibian, A. Winter, S. Paganelli, H. Rieger, and G. Morigi, Phys. Rev. Lett. **110**, 075304 (2013).
[28] N. Dogra, F. Brennecke, S. D. Huber, and T. Donner, Phys. Rev. A **94**, 023632 (2016).
[29] A. E. Niederle, G. Morigi, and H. Rieger, Phys. Rev. A **94**, 033607 (2016).
[30] M. P. A. Fisher, P. B. Weichman, G. Grinstein, and D. S. Fisher, Phys. Rev. B **40**, 546 (1989).
[31] Y. Li, L. He, and W. Hofstetter, Phys. Rev. A **87**, 051604(R) (2013).
[32] S. F. Caballero-Benitez and I. B. Mekhov, Phys. Rev. Lett. **115**, 243604 (2015).
[33] S. F. Caballero-Benitez and I. B. Mekhov, New J. Phys. **18**, 113010 (2016).

[34] T. Flottat, L. de Forges de Parny, F. Hébert, V. G. Rousseau, and G. G. Batrouni, Phys. Rev. B **95**, 144501 (2017).
[35] L. Himbert, C. Cormick, R. Kraus, S. Sharma, and G. Morigi, Phys. Rev. A **99**, 043633 (2019).
[36] P. Sierant, K. Biedroń, G. Morigi, and J. Zakrzewski, SciPost Phys. **7**, 8 (2019).
[37] T. Dauxois, P. de Buyl, L. Lori, and S. Ruffo, J. Stat. Mech. (2010) P06015.
[38] R. Frésard, arXiv:cond-mat/9405053.
[39] See Supplemental Material at http://link.aps.org/supplemental/10.1103/PhysRevLett.129.143001 for: (1) a detailed description of the slave-boson theory for the extended Bose-Hubbard model; (2) Further numerical studies of EE across the phase transitions with commensurate and incommensurate fillings; (3) the slave-boson study of the entanglement in the LMG model, which includes Refs. [9,11,24–26,40–42].
[40] I. Frérot and T. Roscilde, Phys. Rev. B **92**, 115129 (2015).
[41] J. Blaizot and G. Ripka, *Quantum Theory of Finite Systems* (The MIT Press, Cambridge, MA, 1986).
[42] H. F. Song, S. Rachel, and K. Le Hur, Phys. Rev. B **82**, 012405 (2010).
[43] S. D. Huber, E. Altman, H. P. Büchler, and G. Blatter, Phys. Rev. B **75**, 085106 (2007).
[44] This treatment is required to get meaningful results for the EE in the SF phase. We apply a field term coupling directly to the bosonic field [see SM [39]] and scaling like the N^{-2} that introduces a gap in the excitation spectrum scaling as N^{-1}, in agreement with what is expected for systems breaking a $U(1)$ symmetry [40].
[45] S. B. Jäger, J. Cooper, M. J. Holland, and G. Morigi, Phys. Rev. Lett. **123**, 053601 (2019).
[46] K. Seetharam, A. Lerose, R. Fazio, and J. Marino, Phys. Rev. Research **4**, 013089 (2022).
[47] P. Deuar, A. Ferrier, M. Matuszewski, G. Orso, and M. H. Szymańska, PRX Quantum **2**, 010319 (2021).
[48] C. Gross and W. S. Bakr, Nat. Phys. **17**, 1316 (2021).
[49] R. Islam, R. Ma, P. M. Preiss, M. Eric Tai, A. Lukin, M. Rispoli, and M. Greiner, Nature (London) **528**, 77 (2015).
[50] T. Brydges, A. Elben, P. Jurcevic, B. Vermersch, C. Maier, B. P. Lanyon, P. Zoller, R. Blatt, and C. F. Roos, Science **364**, 260 (2019).